LA-UR- 98-1355

CONF-981054--

Approved for public release; distribution is unlimited.

Title: MODELING OF THE RECRYSTALLIZATION TEXTURES OF Al-ALLOYS AFTE HOT DEFORMATION

Author(s): Olaf Engler, Hans Erik Vatne

Submitted to: Hot Deformation of Al-Alloys II, TMS Meeting
Rosemont, IL
10/11-15/1998

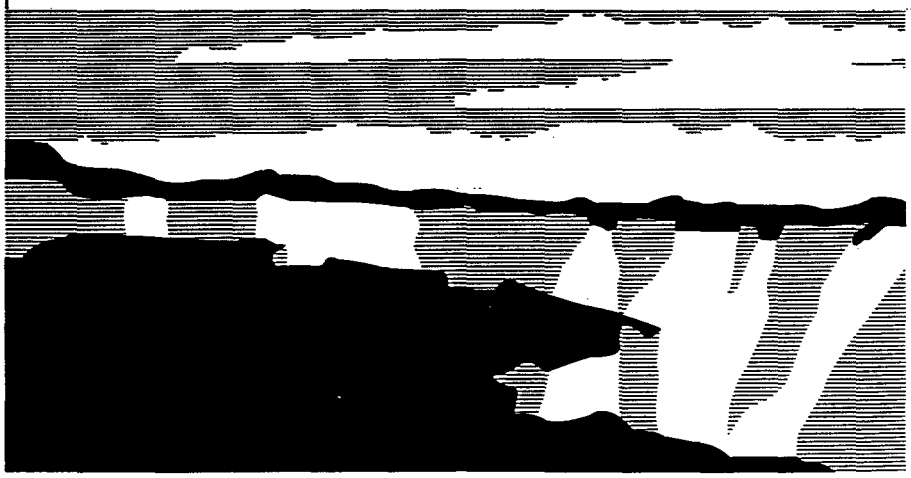

Los Alamos
NATIONAL LABORATORY

DISCLAIMER

DISCLAIMER

Portions of this document may be illegible in electronic image products. Images are produced from the best available original document.

LA-UR- 98-1355

JOM – 25-Mar-98

Modeling of the Recrystallization Textures of Al-Alloys after Hot Deformation

O. Engler[1]), H.E. Vatne[2])

[1]) Los Alamos National Laboratory, Center for Materials Science, Mail Stop K765, Los Alamos, NM 87545, USA

[2]) Hydro Aluminium, R&D Centre Sunndalsøra, N–6601 Sunndalsøra, Norway

ABSTRACT

The recrystallization textures of Al-alloys can be explained by a growth selection of grains with an approximate 40°<111> orientation relationship out of a limited spectrum of preferentially formed nucleus orientations. Accordingly, recrystallization textures can be modeled by the multiplication of a function $f(g)^{nucl}$ describing the probability of nucleation of the various orientations with a function $f(g)^{grow}$ representing their growth probability.

Whereas the growth probability can be accounted for by a 40°<111> transformation of the rolling texture, the nucleation probability of the respective grains is given by the distribution of potential nucleus orientations, which is known from local texture analysis for the most important nucleation sites in rolled Al-alloys, cube-bands, grain boundaries and second-phase particles. The contribution of each of these nucleation sites are determined according to an approach to calculate the number of nuclei forming at each nucleation site, which is based on microstructural investigations on the evolution of the various nucleation sites during deformation.

The paper describes the model for recrystallization texture simulation in Al-alloys and gives examples of recrystallization textures of AA3004 deformed in plane strain compression at a variety of different deformation temperatures and strain rates.

INTRODUCTION

During thermomechanical processing of Al-alloys control of crystallographic texture and grain size in the final sheet product is a vital step. Texture is of importance in controlling mechanical anisotropy – e.g. the earing behavior – which affects the forming properties of sheet products. A too large grain size is detrimental with regard to mechanical properties, and it can also cause undesired surface effects (orange peel). Thus, modeling of the evolution of microstructure and texture during thermomechanical processing is of great interest to predict the properties and so to maintain the quality of the final sheet products. However, whereas in the steel industry modeling of the microstructural processes is a well established tool for optimizing processing conditions [1-3] , in the aluminum-industry modeling is at a much earlier development stage [3-7]. This can mainly be attributed to the much more complex microstructural processes during the recrystallization of Al-alloys: Whereas for modeling of the recrystallization in steels one microstructure parameter (the grain size) proved to be sufficient, in Al-alloys much more influencing parameters have to be taken into account.

After a recrystallization anneal, the textures of most Al-alloys are comprised of three groups of orientations with varying composition [8,9]. As an example, Figure 1 shows the orientation distribution function (ODF) of commercial purity Al (AA1145) after cold rolling and subsequent recrystallization, presented in sections through the three-dimensional orientation space defined by the Euler angles φ_1, Φ, φ_2 [10]. The recrystallization textures of most Al-alloys – especially after hot deformation – are dominated by a strong cube-orientation {001}<100> with pronounced scatter about the rolling direction towards Goss={011}<100>. Additionally, an R-orientation comprising all orientations close to the former rolling texture is often observed, which is particularly pronounced in the recrystallization textures of cold deformed Fe-containing Al-alloys. Besides of these two quite well-defined recrystallization texture components, the ODFs typically comprise a more or less strong background – the random 'component' – which mainly affects the texture sharpness. It is clear that a meaningful recrystallization model has to properly simulate these orientations as well as their respective amounts in the recrystallization textures.

Although for many years the texture changes during recrystallization have been explained in terms of one out of the two rivaling theories of oriented nucleation and growth selection [11], an interpretation of recrystallization textures solely based on either of them commonly fails. Recent experimental investigations – in particular with the help of electron back scattering diffraction

(EBSD) to determine the crystallographic orientations of small regions down to sub-micrometer size in an SEM – have provided new insight into the mechanisms of nucleation and growth of recrystallization and, hence, into the evolution of microstructure and texture during recrystallization in dependence on both processing and microstructural parameters. As a result of those studies it is now widely accepted that the recrystallization textures of Al-alloys evolve by a preferred formation of some orientations at characteristic nucleation sites and a subsequent growth selection of distinct orientations out of this spectrum of nucleus orientations.

Nucleation of recrystallization takes place by enhanced subgrain growth in the vicinity of structural heterogeneities, and in commercially rolled Al-alloys three main nucleation sites have been identified – cube-bands, grain boundaries and large second-phase particles [12-14]. For each of these characteristic nucleation sites a specific spectrum of preferentially formed nucleus orientations has be established, which can be used for a recrystallization texture simulation.

During the subsequent *growth* of the recrystallized grains, it has been shown that the orientations of the fastest growing grains can often be related to the rolling texture by a 40°<111> rotation [15], which is attributed to a (micro-) growth selection of such preferably oriented grains [14,16,17]. Therefore – although the underlying reasons for the preference of this orientation relationship are not completely understood so far – a model to simulate the recrystallization texture of Al-alloys has to take the 40°<111> growth selection into account.

Based on this presupposition – a growth selection of orientations with a 40<111> orientation relationship out of a distinct, limited spectrum of preferentially formed nucleus orientations – a new model to simulate the recrystallization textures of Al-alloys has been developed. This paper is aimed to outline the basic ideas of the model which is based on two complementary approaches by the present authors [18,19]. In order to demonstrate the predictive power of the model, simulation results which pertain to a variation of strain rate and deformation temperature in the Al-alloy AA3004 are presented. More details on the model as well as further simulations pertaining to recrystallization of cold deformed Al-alloys will be given in a separate paper [20].

THE MODEL

The model approach

In the case of a growth selection of some orientations out of a limited spectrum of preferentially formed nucleus orientations the probability of a given orientation to form during recrystallization is given by the probability of its nucleation and the probability of its subsequent growth [21,22]. With this basic premise, recrystallization textures can be modeled by multiplication of a function $f(g)^{nucl}$ representing the probability of the nucleation of the new grains with their growth probability function $f(g)^{grow}$ (Figure 2) [18]:

$$f(g)^{sim} = f(g)^{nucl} \cdot f(g)^{grow} \tag{1}$$

The ODF is defined as a function describing the intensity or *probability* with which a given orientation appears in the corresponding texture. Therefore, the probability of nucleation can be derived from the orientation distribution of the potential nuclei, which can e.g. be obtained by EBSD-local texture measurements at the potential nucleation sites [18]. However, detailed EBSD-analysis of the potential nucleus orientations is an extremely time-consuming procedure which is certainly not suitable for large-scale texture simulations. Therefore, based on the current understanding on the mechanisms of recrystallization nucleation in Al-alloys, for either nucleation site generic nucleus orientation distributions $f(g)^{nucl}_{Cube}$, $f(g)^{nucl}_{GB}$ and $f(g)^{nucl}_{PSN}$ were generated, where the functions $f(g)^{nucl}_{Cube}$, $f(g)^{nucl}_{GB}$ and $f(g)^{nucl}_{PSN}$ respectively denote the characteristic orientation spectra of the cube-bands, grain boundaries and particles. In order to take the simultaneous nucleation at different nucleation sites into account, the nucleation distribution function $f(g)^{nucl}$ is derived by weighting the contributions of the different nucleation sites:

$$f(g)^{nucl} = x_{Cube} \cdot f(g)^{nucl}_{Cube} + x_{GB} \cdot f(g)^{nucl}_{GB} + x_{PSN} \cdot f(g)^{nucl}_{PSN} \tag{2}$$

The weight factors x_i denote the probability or efficiency of nucleation at the corresponding nucleation sites. They can be derived according to a recent approach to calculate the number of nuclei N_i forming at each nucleation site, which is based on experimental investigations on the nature and particularly on the evolution of the various nucleation sites during the preceding deformation [19]. With an appropriate normalization, the numbers of nuclei N_i can readily be transformed into the weight factors x_i.

The growth probability function $f(g)^{grow}$ must consider the preference of nuclei with a 40°<111> orientation relationship to the deformed matrix. It turned out that a numerical rotation of the corresponding rolling texture by 40° about all possible <111>-axes gives satisfactory results [18].

Finally, the nucleation and the growth probabilities are multiplied to yield the simulated recrystallization texture $f(g)^{sim}$ (Equation 1, Figure 2), which can then be plotted and compared to the corresponding experimental recrystallization texture. In the following sections, the characteristic nucleus distribution functions $f(g)^{nucl}$ and the principles to determine the weight factors x_i will briefly be outlined; more details on the underlying model approaches can be found elsewhere [18,19].

Nucleation at cube-bands

Nucleation of cube-oriented grains is known to take place in the so-called cube-bands, band-like structures that are part of the as-deformed microstructure [12,23,24]. In the present model, the number of cube-oriented nuclei N_{Cube} is derived from the volume M_{Cube} of cube-oriented subgrains within these cube-bands, the boundary area A between cube-bands and surrounding matrix, and the fraction S^*_{Cube} of cube-subgrains which exceed the critical size for nucleation δ*:

$$N_{Cube} = c_{Cube} \frac{A(\varepsilon)\, M_{Cube}(\varepsilon)\, S^*_{Cube}}{\delta^2_{Cube}} \qquad (3)$$

(c_{Cube}: modeling constant describing the efficiency of nucleation at cube-bands; see below). δ_{Cube} is the average subgrain size within the cube-bands which – in accordance with detailed experimental observations – has been assumed to be 1.5 times larger than the average subgrain size in the matrix δ. Thorough experimental investigations about the evolution of cube-bands in hot deformed Al-alloys strongly suggest that the cube-bands are deformed 'old' cube-grains which retained their original cube-orientation of the initial state [23-26]. Hence, the volume of cube-orientation in the cube-bands M_{Cube} is computed from the initial volume fraction M^0_{Cube} under consideration of the deformation parameters strain ε, deformation temperature T_D and strain rate $\dot{\varepsilon}$ [18,19]. The area A between the cube-bands and the surrounding matrix and their increase with strain ε can be deduced by simple geometrical considerations from the initial grain size D_0 and

the strain ε. The number S^*_{Cube} of overcritically large cube-subgrains with size exceeding δ* can be derived from integration of the subgrain size distribution function $f_{\mathrm{Cube}}(\delta)$ [19].

With regard to the orientation distribution of nuclei forming in the cube-bands, detailed local texture analysis of the subgrains within the cube-bands as well as the grains that evolve out of the cube-bands yielded the cube-orientation with strong rotations either around the rolling direction or, less pronounced, about the transverse direction [14,26,27]. Accordingly, the synthesized orientation spectrum for nuclei forming in cube-bands, i.e. the nucleus orientation distribution $f(g)^{nucl}_{Cube}$, consists of the cube-orientation and its rotations [20].

Nucleation at grain boundaries

Besides the cube-bands, the large-angle grain boundaries between the deformed grains can act as viable nucleation sites. For the number of nuclei forming at the grain boundaries considerations analogous to the cube-bands yield a density of nucleation sites N_{GB} of:

$$N_{GB} = c_{GB} \frac{A(\varepsilon)(1 - M_{Cube}) S^*_{GB}}{\delta^2} \tag{4}$$

(c_{GB}: modeling constant describing the efficiency of nucleation at grain boundaries).

There is still a dispute on the orientations of the new grains that form at the grain boundaries. Whereas some publications report on randomly oriented grains [13,28], in other investigations orientation distributions close to the corresponding deformation texture – though weaker with noticeably larger scatter – have been reported [14,17,29,30]. In the present calculations, the nucleus spectrum $f(g)^{nucl}_{GB}$ is derived from the respective rolling texture with an artificial weakening (randomizing) according to:

$$f(g)^{nucl}_{GB} = \frac{x_{GB}}{2} \cdot f(g)^{def} + \frac{x_{GB}}{2} \cdot 1 \tag{5}$$

Particle stimulated nucleation (PSN)

Particle stimulated nucleation (PSN) takes place in the turbulent zones that form around large particles to accommodate deformation incompatibilities, i.e. in the so-called deformation zones [31]. As the maximum possible nucleus size is limited to the size of the deformation zones λ, which again is linked to the particle size η, a critical particle size η* for successful nucleation can be expressed as:

$$\eta^* \approx \frac{\lambda}{2} = \frac{1}{2} \cdot \frac{4 \cdot \gamma_{GB}}{p_D} \tag{6}$$

(γ_{GB}: specific grain boundary energy, p_D: driving force for recrystallization). The density of PSN-sites, N_{PSN}, is determined by integration over the particles size distribution $f(\eta)$ starting from particles with size η^*. In most commercial Al-alloys, the distribution of large particles follows an exponential relationship with the characteristic distribution parameters N_0 and L [32], so that the density of PSN-sites becomes:

$$N_{PSN} = c_{PSN}\, N_0 \exp\left(-\frac{2L\gamma_{GB}}{p_D}\right) \tag{7}$$

(c_{PSN}: modeling constant describing the efficiency of PSN).

Because of the strong interactions between dislocations and particles the subgrain orientations within the deformation zones – i.e. the potential nucleation sites – are subjected to strong rotations. Accordingly, often an entirely random orientation distribution of the deformation zones has been reported [31,33], which means that the nucleation probability $f(g)_{PSN}^{nucl}$ would be 1 [18]. However, thorough investigations of the local orientations within the deformation zones proved that they are related to the surrounding matrix by an approximate <112>-rotation, which is caused by the dislocation slip activities [34]. In accordance with these findings, slightly better coincidence of model predictions and experimental results could be achieved by a weighted 35°<112>-transformation of the rolling texture to obtain the nucleus orientation distribution $f(g)_{PSN}^{nucl}$ [35].

Driving force

To derive the weight factors x_i as described above the driving force for recrystallization p_D and the subgrain size δ must be known. In Al-alloys that are composed of a subgrain structure the driving force is composed of two contributions, the energy stored in the subgrain boundaries and the energy of the dislocations in the subgrain interior:

$$p_D = \frac{\alpha \gamma_{SB}}{\delta} + \frac{1}{2}\mu b^2 \cdot \rho \tag{8}$$

(α: geometric constant of the order of 3, γ_{SB}: specific subgrain boundary energy, μ: shear modulus, b: Burgers-vector). The dislocation density within the subgrains, ρ, and the average

subgrain size, δ, have been found to be linked trough the relation $\sqrt{\rho} = C/\delta$, where C is a constant of the order of 2 for hot deformed AA3004 [19]. Both the subgrain boundary energy γ_{SB} and the energy of an ordinary large-angle grain boundary γ_{GB} can be expressed in terms of the well-known Read-Shockley-relation, so that the driving force p_D can be written as:

$$p_D = \frac{\alpha \gamma_{GB} \theta}{\delta \theta_C} \ln\left(\frac{e\theta_C}{\theta}\right) + \frac{C^2 \mu b^2}{2\delta^2} \tag{9}$$

θ and θ_C respectively denote the average and the maximum angle between neighboring subgrains at a subgrain boundary. Whereas θ_C is usually estimated to be 15°, θ varies with strain ε according to $\theta = 3° - \exp(-3\varepsilon)$.

After cold deformation, the evolution of the average subgrain size δ with strain ε can be estimated from the following empirical relation:

$$\delta = 3.5 \cdot 10^{-7} + 1.7 \cdot 10^{-7} / \varepsilon \ [m] \tag{10}$$

However, after hot deformation the influence of the deformation parameters deformation temperature T_D and strain rate $\dot{\varepsilon}$ on the subgrain size has to be considered, as discussed in detail by Vatne et al. [19]:

$$\frac{1}{\delta} = \frac{kT_D}{A^*} \ln\left(\frac{Z\delta^2}{B^*}\right) \tag{11}$$

(k: Boltzmann constant, A^*, B^*: alloy-dependent constants). In this equation, the Zener-Hollomon parameter Z takes the opposite effects of T_D and $\dot{\varepsilon}$ into account:

$$Z = \dot{\varepsilon} \exp\left(\frac{Q}{kT_D}\right) \tag{12}$$

The activation energy Q was chosen to $156kJ/mol$ ($1.62eV$) throughout the present calculations.

Grain size

With the numbers of nuclei forming at the various nucleation sites, the final recrystallized grain size D_{RX} can be estimated by:

$$D_{RX} = \frac{G}{\left(N_{PSN} + N_{Cube} + N_{GB}\right)^{1/3}} \tag{13}$$

where G is a modeling constant representing a growth efficiency.

APPLICATION OF THE MODEL

The present model to simulate recrystallization textures is based on a thorough description of the evolution of the microstructure – especially of the nucleation sites – during the deformation of the material prior to recrystallization. For that purpose, the processing parameters strain ε, strain rate $\dot{\varepsilon}$ and deformation temperature T_D as well as the texture in the as-deformed state must be known. Furthermore, several parameters to characterize the microstructure prior to the deformation have to be determined, namely the initial grain size D_0, the initial fraction of cube-oriented grains M_0, and the parameters L and N_0 which describe the particle size distribution. In the next step, the model constants c_{Cube}, c_{GB}, and c_{PSN} describing the efficiency of nucleation at the respective nucleation sites are determined by a fitting procedure. As these modeling constants c_i only depend on the alloy, fitting of one of the experimental recrystallization textures is sufficient and with this set of modeling constants the model is able to predict recrystallization textures within a given range of experimental parameters for this alloy. Finally, the model can be run to perform the rolling texture transformations and to derive the weight factors x_i and, therewith, the recrystallization textures can be simulated.

In order to study to what extent the model can account for the influence of the processing parameters during hot deformation on the resulting recrystallization textures, samples of the Al-Mn-Mg alloy AA3004 were deformed in plane strain compression (PSC) to strain ε=1 at different deformation temperatures T_D and strain rates $\dot{\varepsilon}$, i.e. at different values of the Zener Hollomon parameter Z (Eq. 12) [36]. Subsequently, the samples were recrystallization annealed for 30s at 430°C.

It turned out that both the texture and the microstructure results could be linked to the deformation parameters in form of the Zener Hollomon parameter Z. To illustrate this, Figure 3 shows the recrystallization textures of two samples, which were deformed respectively at a low value of $Z=5.3\cdot10^{12}s^{-1}$ and a high value of $Z=3.9\cdot10^{16}s^{-1}$. After the recrystallization of the samples that were deformed at low Z-values, i.e. high T_D and/or low $\dot{\varepsilon}$, typical cube-textures formed (Figure 3a), although because of the low level of deformation the textures were quite weak. The recrystallized grain size was about 30μm with the grains being slightly elongated in the rolling direction. In the samples deformed at high Z, i.e. low T_D and/or high $\dot{\varepsilon}$, in contrast, very fine grained equiaxed microstructures (~20μm) and very weak, virtually random, recrystallization textures were obtained (Figure 3b). Figure 4 summarizes these findings in terms of the volume

fraction of the cube-orientation and the grain size in dependence on the Zener-Hollomon parameter Z. In accordance with earlier investigations, it is concluded that with decreasing Z PSN becomes less effective, whereas nucleation at the cube-bands is favored, so that the cube-oriented grains increasingly dominate the recrystallization textures.

In order to assess the capability of the present model of accounting for the influence of the deformation parameters T_D and $\dot{\varepsilon}$ on the recrystallization, the resulting recrystallization textures have been simulated. The necessary input data for M^0_{Cube}, D_0 and the particle size distribution parameters N_0 and L as well as the experimental rolling and recrystallization textures were taken from an earlier paper [36]. Figure 5 shows the model predictions in terms of the evolution of the weight factors x_i and the grain size D_{RX} with Zener-Hollomon parameter Z, which were obtained with the modeling constants c_{PSN}=1.0, c_{Cube}=0.4 and c_{GB}=0.25. These data were then used to simulate the recrystallization textures; and Figure 6 shows the modeled textures of the two examples presented in Figure 3, indicating very good agreement between both. It turned out that x_{PSN} strongly increased from about 0 to values exceeding 0.9 with increasing Z, which reflects the strong dependence of the stored energy of recrystallization on the Zener-Hollomon parameter Z (Eqs. 9-12). Accordingly, x_{Cube} and x_{GB} decreased, although the corresponding nucleation site numbers, N_{Cube} and N_{GB}, happened to increase slightly. This strong increase in the total number of nucleation sites N_i gave rise to the strong decrease in the final recrystallized grain size D_{RX} with increasing Z, which is in very good agreement with the experimental data (Figure 4).

To compare simulated and experimental recrystallization textures, instead of plotting the entire ODFs for all cases, the data were condensed by representing the maximum overall texture intensity $f(g)_{max}$ as well as the ND-scatter of the cube-orientation (Figure 7). For the latter, the angle ψ at which the cube-peak had dropped to half intensity was determined. It is obvious that the model simulates the main features of the recrystallization textures very satisfactorily by reproducing the shift from the cube-recrystallization texture towards the PSN-texture as well as the simultaneous texture weakening with increasing Z.

SUMMARY AND CONCLUSIONS

Based on the assumption that recrystallization textures in rolled Al-alloys evolve by a growth selection of 40°<111>-oriented grains out of a limited spectrum of preferentially formed nucleus orientations, the recrystallization textures can be simulated by the multiplication of the probability of nucleation $f(g)^{nucl}$ of the orientations with the probability of their growth $f(g)^{grow}$. In extension of an older model [18], the number of nuclei N_i that form at the various nucleation sites, cube-bands, grain boundaries and large second-phase particles, had to be derived to account for the varying contribution of the respective nucleation sites to the final recrystallization textures. For that purpose, an approach to predict the evolution of N_i based on experimental investigations on the nature and evolution of the respective nucleation sites[19] has been incorporated. The combination of these two complementary approaches now permits simulation of the recrystallization textures of Al-alloys in dependence on both microstructural characteristics and processing parameters.

As an example to demonstrate the predictive power of the model, the recrystallization textures of the Al-alloy AA3004 deformed in plane strain compression at a variety of strain rates and deformation temperatures – i.e. at different values of the Zener-Hollomon parameter Z – were simulated. The model provided a very satisfactory simulation of the corresponding recrystallization textures by reproducing the characteristic shift from a cube-recrystallization texture towards a weak texture as obtained in the case of PSN with increasing Z. Thus, the model is able to simulate the recrystallization textures of Al-alloys for a wide range of microstructural characteristics and processing parameters during the thermomechanical processing of Al-alloys, which can be used to predict and eventually to improve the properties of the final Al-sheet products.

Acknowledgments: The authors are grateful to Prof. Dr. E. Nes and Dr. U.F. Kocks for valuable discussions. The work by OE has been supported by the U.S. Department of Energy and by the Alexander von Humboldt-Foundation through a Feodor Lynen Research Fellowship. HEV acknowledges financial support by the European Commission through Brite/Euram contract BREU-CT96-0399.

References

1. C.M. Sellars, *Mater Sci Technol.*, **1** (1985), pp. 325-332.
2. A. Laasraouni and J.J. Jonas, *Metal. Trans.*, **22A** (1991), pp. 151-160.
3. C.M. Sellars, *Mater Sci Technol.*, **6** (1990), pp. 1072-1081.
4. G.C. Reyes and J.H. Beynon, in *Proc. Hot Deformation of Al-Alloys*, eds. T.G. Langdon et al., (Warrendale, PA: TMS, 1991), pp. 491-508.
5. J. Hirsch, K. Karhausen, and R. Kopp, in *Proc. 4th Int. Conf. on Al-Alloys (ICAA4)*, eds. T.H. Sanders and E.A. Starke, (Atlanta, GA: Georgia Inst. of Tech., 1994), Vol. I, pp. 476-483.
6. C.M. Sellars, F.J. Humphreys, E. Nes, and D. Juul Jensen, in *Proc. 15th Risø Int. Symp.*, eds. S.I. Andersen et al., (Roskilde: Risø Nat. Lab., 1994), pp. 109-133
7. H.E. Vatne, K. Marthinsen, R. Ørsund, and E. Nes, *Metall. Trans.*, **27A** (1996), pp. 4133-4144.
8. D. Juul Jensen, N. Hansen, and F.J. Humphreys, *Acta metall.*, **33** (1985), pp. 2155-2162.
9. O. Engler, H.E. Vatne, and E. Nes, *Mat. Sci. Eng.*, **A205** (1996), pp.187-198.
10. H.J. Bunge, *Texture Analysis in Materials Science*, (London: Butterworths 1982).
11. R.D. Doherty, G. Gottstein, J.R. Hirsch, W.B. Hutchinson, K. Lücke, E. Nes, and P.J. Wilbrandt, in *Proc. ICOTOM 8*, eds. J.S. Kallend and G. Gottstein, (Warrendale, PA: TMS, 1988), pp. 563-572.
12. J. Hjelen, R. Ørsund, and E. Nes, *Acta metall. mater.*, **39** (1991), pp. 1377-1404.
13. H. Weiland, T.N. Rouns, and J. Liu, *Z. Metallk.*, **85** (1994), pp. 592-597.
14. O. Engler, *Mat. Sci. Tech.*, **12** (1996), pp. 859-872.
15. K. Lücke, *Canad. Metall. Quart.*, **13** (1974), pp. 261-274.
16. D. Juul Jensen, *Acta metall. mater.*, **43** (1995), pp. 4117-4129.
17. O. Engler, *Acta mater.*, **46** (1998), pp. 1555-1568.
18. O. Engler, *Textures and Microstructures,* **28** (1997), pp. 197-209.
19. H.E. Vatne, T. Furu, R. Ørsund, and E. Nes, *Acta mater.*, **44** (1996), pp. 4463-4473.
20. O. Engler, *Textures and Microstructures,* (1998), in press.
21. U. Köhler, E. Dahlem-Klein, H. Klein, and H.J. Bunge, *Textures and Microstructures,* **19** (1992), pp. 125-145.
22. J.J. Jonas, L.S. Tóth, and T. Urabe, *Mat. Sci. Forum,* **157-162** (1994), pp. 1713-1730.
23. H. Weiland, and J. Hirsch, *Textures and Microstructures,* **14-18** (1991), pp. 647-652.
24. R.D. Doherty, I. Samajdar, C.T. Necker, H.E. Vatne, and E. Nes, in *Proc. 16th Risø Int. Symp.*, eds. N. Hansen et al., (Roskilde: Risø Nat. Lab., 1995), pp. 1-23.
25. O. Daaland, and E. Nes, *Acta mater.*, **44** (1996), pp. 1389-1411

26. H.E. Vatne, R. Shahani, and E. Nes, *Acta mater.*, **44** (1996), pp. 4447-4462

27. O. Engler, P. Yang, and X.W. Kong, *Acta metall. mater.*, **44** (1996), pp. 3349-3369.

28. H.E. Vatne, S. Benum, R. Shahani, and E. Nes, in *Proc. 16th Risø Int. Symp.*, eds. N. Hansen et al., (Roskilde: Risø Nat. Lab., 1995), pp. 573-579.

29. S.P. Bellier, and R.D. Doherty, *Acta metall.*, **25** (1977), pp. 521-538.

30. W.B. Hutchinson, *Acta metall.*, **37** (1989), pp. 1047-1056.

31. F.J. Humphreys, *Acta metall.*, **25** (1977), pp. 1323-1344.

32. Nes, E. and Hutchinson, W.B., in *Proc. 10th Risø Int. Symp.*, eds. J.B. Bilde-Sørensen et al., (Roskilde: Risø Nat. Lab., 1989), pp. 233-249.

33. A. Oscarsson, *Textures and Microstructures,* **14-18** (1991), pp. 477-482.

34. O. Engler, X.W. Kong, and P. Yang, *Scripta mater.*, **37** (1997), pp. 1665-1674.

35. O. Engler, *Scripta mater.*, **37** (1997), pp. 1675-1683.

36. O. Engler, B. Mülders, and J. Hirsch, *Z. Metallk.*, **87** (1996), pp. 454-464.

Figure captions

Figure 1: Recrystallization texture of commercial purity Al (AA1145, 95% cold rolled, annealed for 1000s at 350°C).

Figure 2: Scheme of the model.

Figure 3: Experimental recrystallization texture of AA3004 in dependence on the Zener-Hollomon parameter Z (PSC, ε=1, recrystallization annealed for 30s at 430°C).

Figure 4: Evolution of the recrystallized grain size and the volume fraction of the cube-orientation M_{Cube} with the Zener-Hollomon parameter Z (PSC-samples).

Figure 5: Evolution of the weight factors x_i in dependence on the Zener-Hollomon parameter Z.

Figure 6: Modeled recrystallization texture of AA3004 in dependence on the Zener-Hollomon parameter Z (see Figure 3).

Figure 7: Comparison of model and experimental results

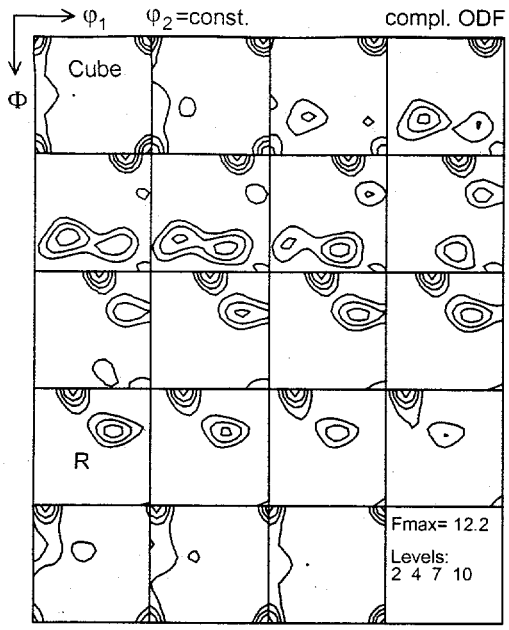

Figure 1: Recrystallization texture of commercial purity Al (AA1145, 95% cold rolled, annealed for 1000s at 350°C).

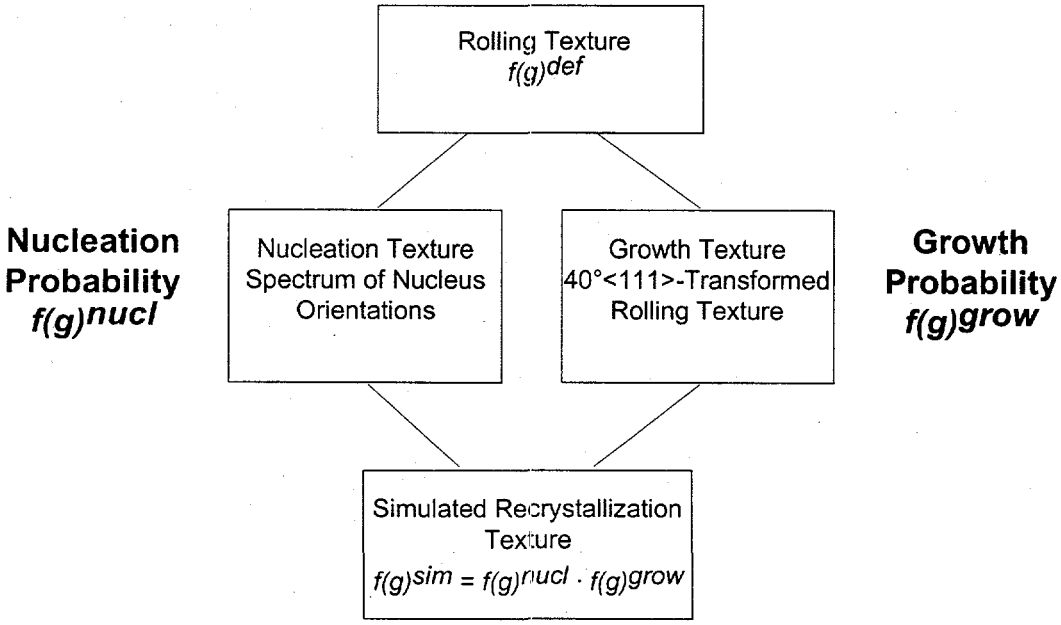

Figure 2: Scheme of the model.

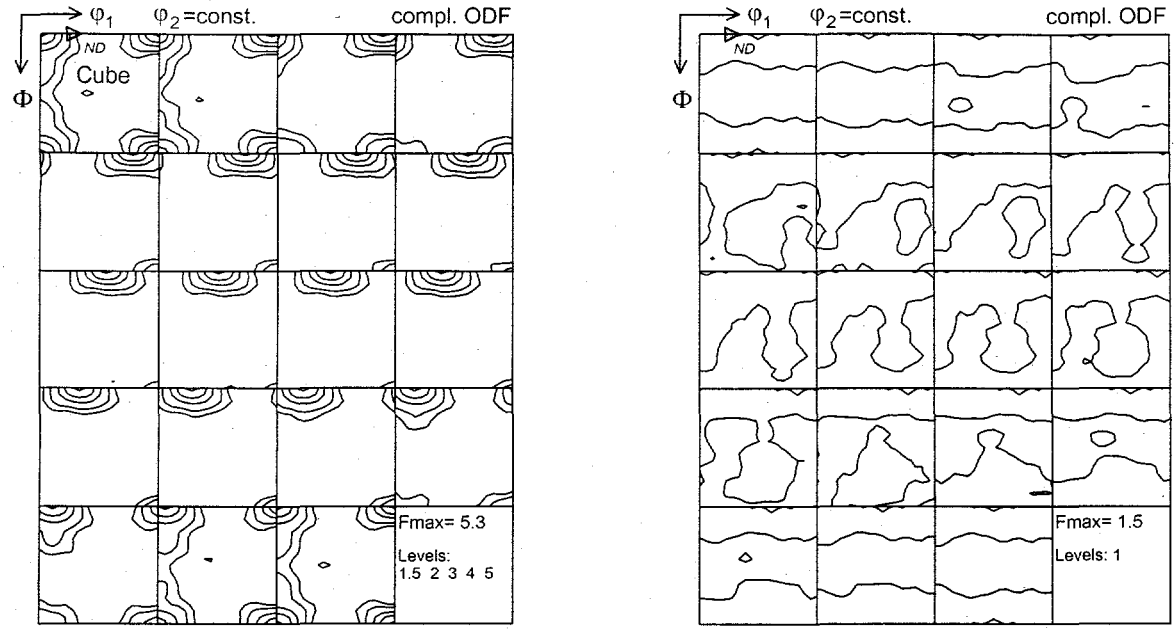

(a) $Z=5.3\cdot10^{12}s^{-1}$, $T_D=245°C$ $\dot{\varepsilon}=10^{-3}s^{-1}$ (b) $Z=3.9\cdot10^{16}s^{-1}$, $T_D=190°C$ $\dot{\varepsilon}=10^{-1}s^{-1}$

Figure 3: Experimental recrystallization texture of AA3004 in dependence on the Zener-Hollomon parameter Z (PSC, ε=1, recrystallization annealed for 30s at 430°C).

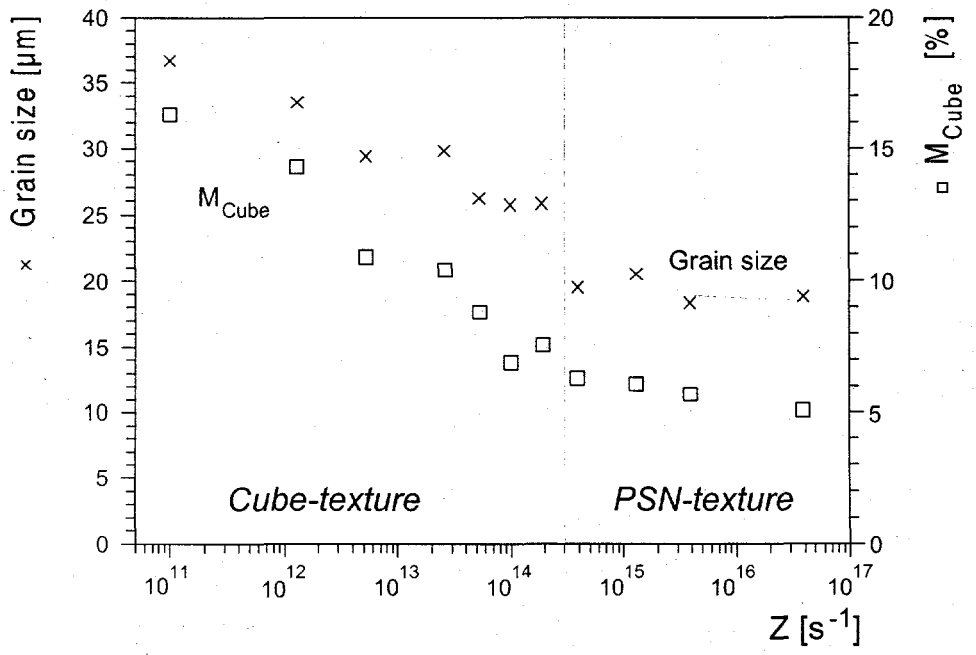

Fig. 4: Evolution of the recrystallized grain size and the volume fraction of the Cube-orientation M_{Cube} with the Zener-Hollomon parameter *Z* (PSC-samples).

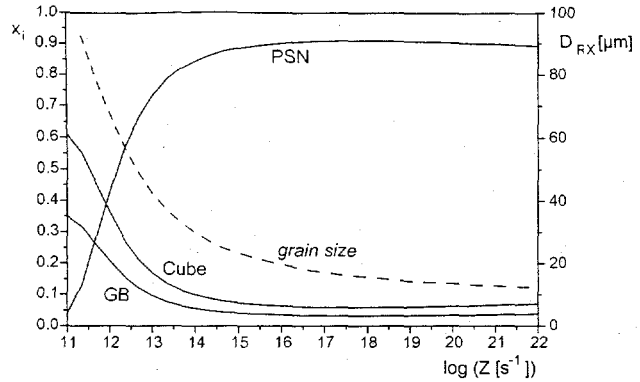

Figure 5: evolution of the weight factors x_i in dependence on the Zener-Hollomon parameter Z.

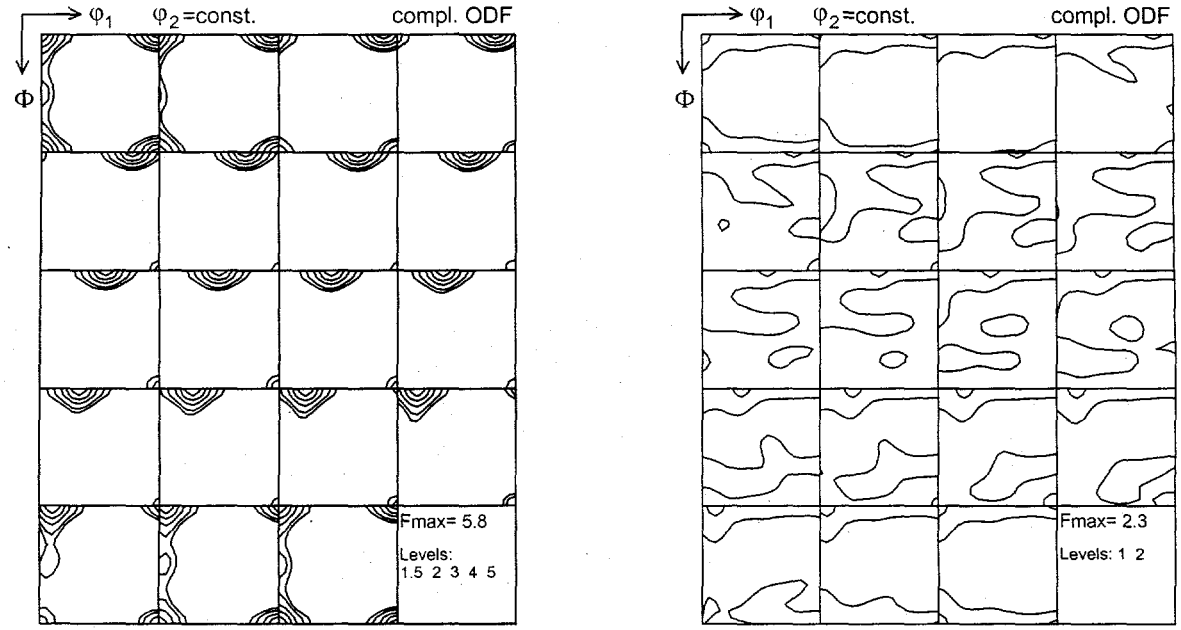

(a) $Z=5.3\cdot10^{12}s^{-1}$, $T_D=245°C$ $\dot{\varepsilon}=10^{-3}s^{-1}$ (b) $Z=3.9\cdot10^{16}s^{-1}$, $T_D=190°C$ $\dot{\varepsilon}=10^{-1}s^{-1}$

Figure 6: Modeled recrystallization texture of AA3004 in dependence on the Zener-Hollomon parameter Z (see Figure 3).

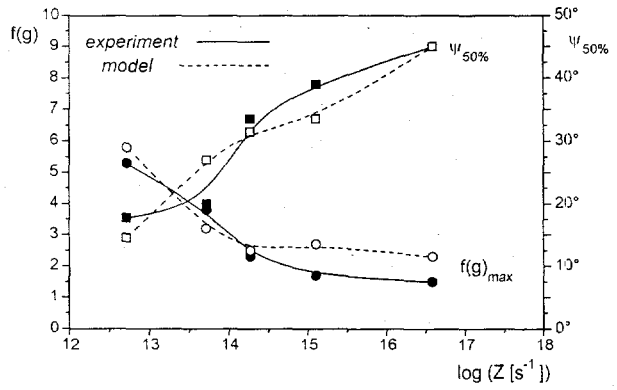

Figure 7: Comparison of model and experimental results